






Penning-trap eigenfrequency measurements with optical radiofrequency detectors

J. Berrocal ¹, A. Hernández,¹ I. Arrazola,² F. Domínguez,¹ A. Carrasco-Sanz ³, F. J. Fernández ⁴,
M. Block ^{5,6,7} and D. Rodríguez ^{1,8,*}

¹Departamento de Física Atómica, Molecular y Nuclear, Universidad de Granada, 18071 Granada, Spain

²Vienna Center for Quantum Science and Technology, Atominstitut, TU Wien, 1040 Vienna, Austria

³Departamento de Óptica, Universidad de Granada, 18071 Granada, Spain

⁴Departamento de Arquitectura y Tecnología de Computadores, Universidad de Granada, 18071 Granada, Spain

⁵Department Chemie - Standort TRIGA, Johannes Gutenberg-Universität Mainz, D-55099 Mainz, Germany

⁶GSI Helmholtzzentrum für Schwerionenforschung GmbH, D-64291 Darmstadt, Germany

⁷Helmholtz-Institut Mainz, D-55099 Mainz, Germany

⁸Centro de Investigación en Tecnologías de la Información y las Comunicaciones, Universidad de Granada, 18071 Granada, Spain



(Received 17 June 2023; revised 8 October 2023; accepted 29 November 2023; published 3 January 2024)

We use an electric-dipole laser-driven transition to precisely measure the cyclotron-frequency ratios of the pairs $^{42}\text{Ca}^+ - ^{40}\text{Ca}^+$, $^{44}\text{Ca}^+ - ^{40}\text{Ca}^+$, and $^{48}\text{Ca}^+ - ^{40}\text{Ca}^+$ in a 7-tesla Penning trap. A single laser-cooled ($T \approx 1$ mK) ion serves, together with photon-counting and photon-imaging units, as a radiofrequency detector covering a broadband frequency spectrum, in the present case from kHz to a few MHz. Such detectors ($^{40,42,44,48}\text{Ca}^+$) allow measuring extremely small forces increasing the sensitivity in Penning-trap mass spectrometry. The direct determination of the ions' amplitudes makes a cyclotron-frequency measurement process more robust against inhomogeneities of the magnetic field and/or deviations of the electric quadrupole field due to mechanical imperfections of the trap.

DOI: [10.1103/PhysRevResearch.6.L012001](https://doi.org/10.1103/PhysRevResearch.6.L012001)

Penning traps have a distinct and unique feature such as the natural presence of a large magnetic field, enabling the stable detection of extremely weak forces and electric fields with many trapped ions [1,2]. In addition, the accurate determination of the cyclotron frequency of a charged (anti)particle confined in the trap can be utilized to evaluate fundamental constants [3], to perform fundamental symmetries tests [4,5], and to search for new Physics [6–9]. Penning-trap single-particle detectors have been developed on the basis of electronic detection following the principle of the stored ion calorimeter [10]. The cyclotron frequency

$$\nu_c = \frac{1}{2\pi} \frac{q}{m} B, \quad (1)$$

directly proportional to the particles' charge-to-mass ratio (q/m), is determined from the measurements of three characteristic frequencies of the target particle [11]. A measurement of the magnetic field strength (B) is avoided by measuring cyclotron-frequency ratios, i.e., alternating the ν_c measurement of the target ion with the ν_c measurement of another charged particle, with well-known q/m [6,12]. In single-ion

Penning-trap experiments carried out to date, the three characteristic frequencies of the ion are determined by damping one of the ion's eigenmotions through a resonant tank circuit at 4 K [13,14]. Thus, one eigenfrequency is obtained directly by Fourier transformation of the induced-current signal, and the remaining ones are obtained in the same way after applying motional conversion [6,15]. In this Letter, we report on direct measurements of the three characteristic frequencies of a single laser-cooled calcium ion in a 7-tesla Penning trap, utilizing the ion as a radiofrequency (rf) fluorescence detector [16–18] covering the range from kHz to MHz. We present the cyclotron-frequency ratios of $^{42}\text{Ca}^+ - ^{40}\text{Ca}^+$, $^{44}\text{Ca}^+ - ^{40}\text{Ca}^+$, and $^{48}\text{Ca}^+ - ^{40}\text{Ca}^+$ from the observation of the fluorescence photons of the $^2S_{1/2} \rightarrow ^2P_{1/2}$ electric-dipole transition in calcium after applying external rf fields. Precise cyclotron-frequency ratios of even calcium isotopes have been used, combined with the mass value of ^{40}Ca [19] and spectroscopy data [20–22], to probe fundamental symmetries, and there is still room for improving the precision.

For a Doppler-cooled ion, a decrease in its temperature from 4 K (electronic detection) to 1 mK (optical detection) directly translates into a reduction of the ion's oscillation amplitude. It is thus sensitive to extremely small forces, and the measurement will be less affected by magnetic field inhomogeneities, imperfections of the electric field, relativistic effects, and induced charges on the trap electrodes. Furthermore, the ion is (optically) observed before and after the external field is applied. This ion-based detector can be utilized in accurate mass spectrometry on any atomic or molecular ion, which cannot be directly laser cooled, when

*danielrodriguez@ugr.es

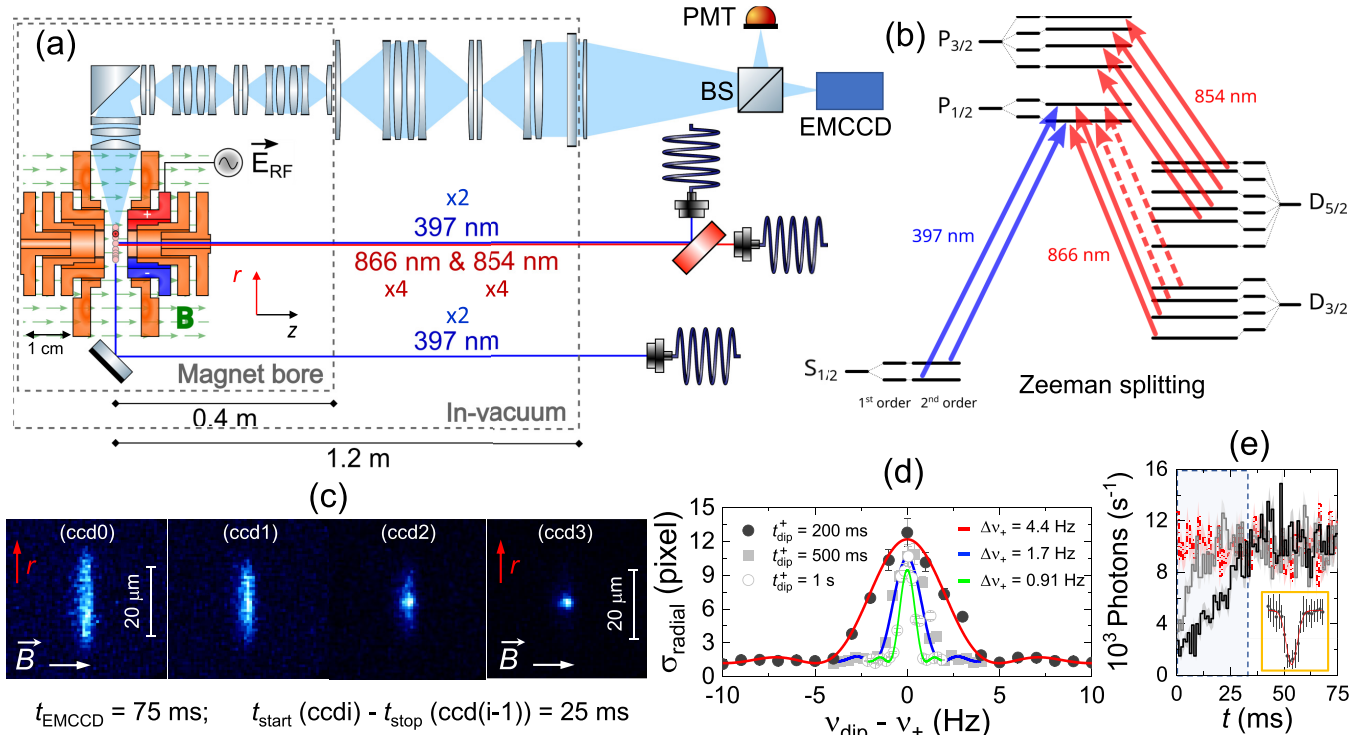


FIG. 1. (a) Sketch showing a longitudinal cut of the open-ring Penning trap [28,29], the dipolar electric field (in the radial direction), and the optical system (not to scale) for photon detection. (b) Level scheme of calcium ions in a strong magnetic field including first- and second-order Zeeman splittings, indicating all the transitions to be driven to perform Doppler cooling. (c) Sequence of EMCCD images of a calcium ion on applying Doppler cooling after probing the modified-cyclotron motion with an external field oscillating at $\nu_{\text{dip}} = \nu_+$. (d) Standard deviation of the Lorentzian fit to the projections along the r direction of EMCCD images [e.g., (c)-ccd0] vs frequency of the external field for three different excitation times. $\Delta\nu$ corresponds to the FWHM of the fitted Rabi sinc function. (e) Number of photons registered by the PMT for three different values of ν_{dip} ; when the oscillating electric field is not resonant with the axial motion (dotted red), when $\nu_{\text{dip}} = \nu_z$ (solid black), and when $\nu_{\text{dip}} = \nu_z + \Delta\nu_z/2$ (solid gray). Inset: the number of photons collected within the time window delimited by the dashed lines vs frequency of the external field around ν_z .

the target and calcium ion are confined in the same potential well of the Penning trap, forming an unbalanced two-ion Coulomb crystal [23,24]. Such a configuration can be used for identification of exotic single particles, such as super-heavy ions, complementing the measurements carried out to date and permitting the extension of the survey in this mass region [25–27]. Motional frequency metrology on any ion species will also be practicable provided the Coulomb crystal is cooled to the ground state of motion [24].

In the Penning trap, the motion of an ion with a given q/m in the homogeneous magnetic field (~ 0.1 ppm within 1 cm³) and under an ideally perfect quadrupolar electrostatic field is depicted as the superposition of three eigenmotions, i.e., one in the axial (z) direction and two in the radial ($x - y$) plane (represented by the subscripts $+$ and $-$), with ideal characteristic frequencies [11],

$$\nu_z = \frac{1}{2\pi} \sqrt{\frac{qU}{md_0^2}}, \quad \nu_{\pm} = \frac{\nu_c}{2} \left[1 \pm \sqrt{1 - 2 \left(\frac{\nu_z}{\nu_c} \right)^2} \right], \quad (2)$$

where U is the trap depth of the electrostatic potential well, and d_0 a geometrical characteristic length of the trap. In the ideal trap [Eq. (2)], deviations in the eigenfrequencies arise from inhomogeneities and fluctuations of U and B , linked to

the geometry of the trap and the stability of the DC power supplies, and of the superconducting solenoid, respectively.

We determine ν_c in this Letter from a direct measurement of the three eigenfrequencies via [11]

$$\nu_c^2 = \nu_+^2 + \nu_z^2 + \nu_-^2. \quad (3)$$

All three eigenmotions can be probed individually with a dipolar electric field applied for a time t_{dip}^u ($u = \pm, z$), with ν_{dip} swept across an ion's eigenfrequency, analogously to a forced harmonic oscillator. Our trap follows a $\nu_+ \gg \nu_z \gg \nu_-$ configuration ($\nu_+ = 2.686$ MHz, $\nu_z = 142$ kHz, and $\nu_- = 3.8$ kHz for ⁴⁰Ca⁺), which mitigates electric-field-related uncertainties.

The experiments reported here have been carried out using a single laser-cooled ion from different calcium isotopes ($A = 40, 42, 44, 48$) in an open-ring 7-tesla Penning trap, shown schematically in Fig. 1(a) [28]. The isotope of interest was produced by photoionization in a Paul trap using two diode lasers at 423 nm (tunable) and 375 nm (free running), by tuning the frequency of the laser driving the ¹S₀ → ¹P₁ transition to that of the target isotope. The ejection from the Paul trap, transport downstream the beam line, and capture into the Penning trap was as described (for ⁴⁰Ca⁺) in Ref. [29]. The voltages applied to the trap electrodes were modified after the capture to

shape the trap potential with the ring electrode set to 0 V. Due to the magnetic field strength of 7 T, 10 lasers with frequencies, tuned for each particular calcium isotope, are needed for Doppler cooling to drive the transitions shown in Fig. 1(b) [28,30]: 2×397 nm for the $^2S_{1/2,\pm 1/2} \rightarrow ^2P_{1/2,\pm 1/2}$ transitions (cooling), 4×866 nm for the $^2D_{3/2,\pm 1/2,\pm 3/2} \rightarrow ^2P_{1/2,\pm 1/2}$ transitions (repumping), and 4×854 nm for the $^2D_{5/2,\pm 1/2,\pm 3/2} \rightarrow ^2P_{3/2,\pm 1/2\pm 3/2}$ transitions (repumping). The frequencies are distributed through 12 laser beams, with two of them in the radial plane [Fig. 1(a)]. The waists of the 397-nm laser beams are 220–320 μm and 500 μm for the radial and axial directions, respectively [29]. In order to speed up the cooling process, the 397-nm lasers are initially red detuned by a few GHz and scanned towards ~ 10 MHz below resonance, yielding a cooling time of about 30 s. During laser cooling, an axialization drive was applied to efficiently cool the magnetron motion [31]. The detection of fluorescence photons from the $^2P_{1/2,\pm 1/2} \rightarrow ^2S_{1/2,\pm 1/2}$ transitions (397 nm) was carried out using two devices simultaneously: an electron-multiplying charge-coupled device (EMCCD) and a photo-multiplier tube (PMT), both at the focal plane of the ~ 2 -m length optical system, at equal distance from a 50:50 beam splitter (BS) [Fig. 1(a)].

While probing any motion (applying the external dipolar field), two laser beams [dashed lines in Fig. 1(b)] are blocked by means of an acoustic-optical modulator (stop cooling), in order to reduce the linewidth and enhance the sensitivity. Axialization is also turned off. In this process, the ion's energy increases until the dipolar electric field is stopped. Then the laser beams interact again with the ion and axialization is turned on, increasing the number of scattered photons until the ion reaches the Doppler limit. The simultaneous cooling of the radial modes implies a cooling rate for this plane that is lower than for the axial direction [29]. The ion's radial amplitude decays exponentially with a time constant of 80(23) ms, which allows direct observation of the excitation using the EMCCD. Figure 1(c) shows a series of images collected within a few-hundred milliseconds after probing the modified-cyclotron motion with $t_{\text{dip}}^+ = 1$ s, from which the initial amplitude (ρ_+) can be extracted. For a similar measurement of the magnetron motion, $t_{\text{dip}}^- = 100$ ms. The resonance curve after excitation of a radial eigenmotion is built by representing the width of the Lorentzian fitting function to the projection of the photons' distribution along the radial direction as a function of ν_{dip}^+ . Figure 1(d) shows three resonance curves with different t_{dip}^+ , scaling the amplitude of the field V_{dip}^+ . The axial eigenmotion had to be excited to amplitudes that are a factor of 3–4 times larger to be sensitive with the PMT [Fig. 1(e)]. Due to the faster cooling, the excitation is not visible with the EMCCD. For the measurement in Fig. 1(e), $t_{\text{dip}}^z = 100$ ms. The resonance curve after excitation is constructed from the number of detected photons [inset of Fig. 1(e)]. The amplitude of the axial motion is estimated as

$$\rho_z = \frac{E_z}{E_+} \frac{\nu_1}{\nu_z} \left(\rho_+ \frac{V_{\text{dip}}^z}{V_{\text{dip}}^+} \frac{t_{\text{dip}}^+}{2t_{\text{dip}}^+} + \rho_- \frac{V_{\text{dip}}^z}{V_{\text{dip}}^-} \frac{t_{\text{dip}}^-}{2t_{\text{dip}}^-} \right), \quad (4)$$

where $\nu_1 = \nu_+ - \nu_-$, and E is the amplitude of the electric field in the center of the trap (from SIMION simulations) [32].

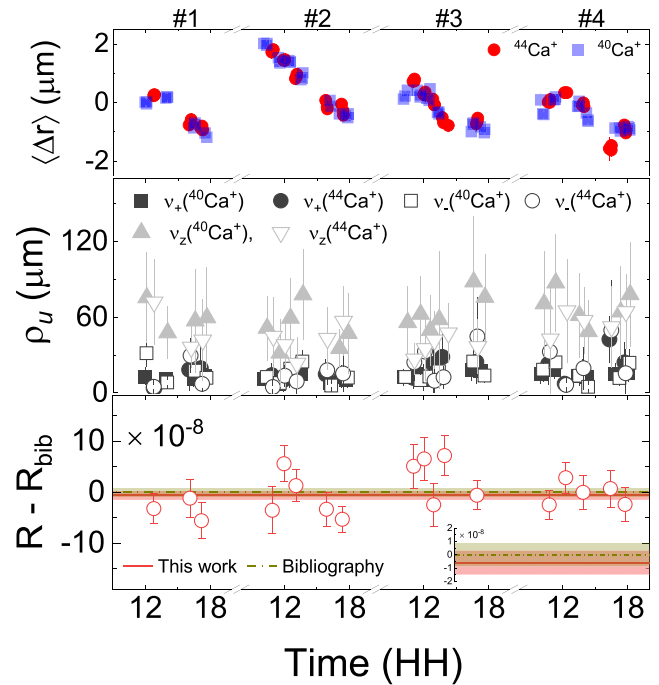


FIG. 2. Four-day measurement of the cyclotron frequencies of $^{40}\text{Ca}^+$ and $^{44}\text{Ca}^+$ including the visualization of the ion motion. Top: Deviation of the center of the ion's photon distribution during the measurements of the radial motions. Middle: Amplitude of the modified-cyclotron ($u = +$), magnetron ($u = -$) and axial ($u = z$) motions during the measurements. Bottom: Comparison between cyclotron-frequency ratios $R = \nu_c(^{40}\text{Ca}^+)/\nu_c(^{44}\text{Ca}^+)$ measured in this work (red empty circles) with the values from the literature [33]. The light-red area (zoomed in the inset) represents the weighted mean value from this work.

We have sequentially measured the cyclotron frequency of a calcium isotope ($A = 42, 44, 48$) and that of $^{40}\text{Ca}^+$. The frequencies of the lasers in Fig. 1(b) were accordingly tuned for each isotope, ranging from a few-hundred MHz to a few GHz. Each measurement of the cyclotron-frequency ratio with this procedure needs about 1 hour, which comprises about 15 minutes per ion and 15 minutes for laser regulation. For a particular isotope, a cyclotron-frequency measurement comprises the measurement of ν_+ , ν_z , and ν_- [Eq. (3)], where the total number of scans was set to about 10/10/5, respectively. For each measurement, the frequency of the external field, ν_{dip} , was swept across resonance and EMCCD images and PMT counts were simultaneously recorded. The time the rf field was applied (t_{dip}^u) and its amplitude (V_{dip}^u) were varied depending on the eigenmotion's envisaged precision. Due to the vacuum conditions and the instabilities of the DC power supplies in the experiments, t_{dip}^+ did not exceed 1 s; in most cases, $t_{\text{dip}}^+ = 500$ ms. t_{dip}^z was typically 100 ms.

Figure 2 shows the cyclotron-frequency ratio $R^{40,44} = \nu_c(^{40}\text{Ca}^+)/\nu_c(^{44}\text{Ca}^+)$ from 18 data points taken during four days of measurements. The positions and amplitudes of the ion are also shown. Our value $R^{40,44} = 1.099\,917\,077\,2(89)$ is in agreement and with the same relative uncertainty as the most accurate value quoted in the literature, $(\delta R/R)^{40,44} = 8.1 \times 10^{-9}$ [33].

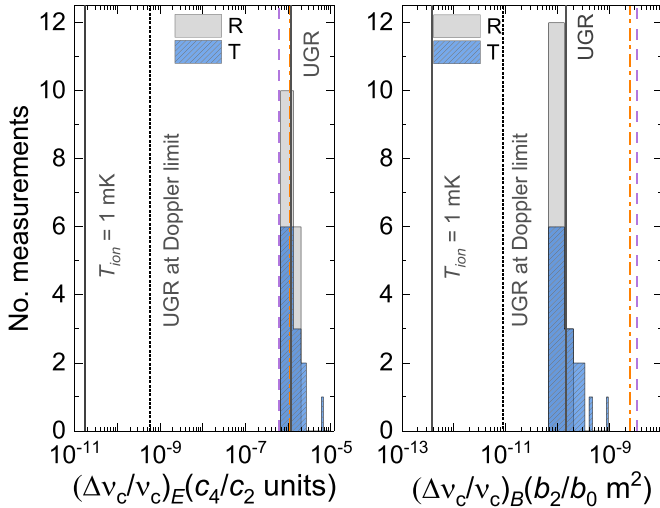


FIG. 3. Relative cyclotron-frequency shifts from the measurements on $^{44}\text{Ca}^+$ (T) and $^{40}\text{Ca}^+$ (R) as a function of ρ_{\pm} (from observations) and ρ_z [Eq. (4)], considering first-order deviations from the ideal quadrupolar field (left) and from an homogeneous magnetic field (right). The histograms are obtained from the data shown in Fig. 2. The solid vertical line is the average of these measurements, the dashed line is the value assumed from experiments at Florida State University [39], and the dash-dotted line is the one from the ion's amplitude in experiments with highly charged ions at the Max-Planck Institute for Nuclear Physics in Heidelberg [40], scaled to an ion with $m/q \sim 40$. The short-dotted lines in both panels (UGR at Doppler limit) indicate our estimated smallest shifts using our technique with the maximum sensitivity in the Doppler limit. The vertical solid lines ($T_{\text{ion}} = 1$ mK) indicate the shifts, providing ρ_u during the measurement is equal to ρ_u at 1 mK.

These measurements were taken with $t_{\text{dip}}^+ = 500$ ms and $t_{\text{dip}}^{z,-} = 100$ ms. The same configuration was utilized for the measurement of the cyclotron-frequency ratio of $^{42}\text{Ca}^+ - ^{40}\text{Ca}^+$, yielding $R^{40,42} = 1.049\,948\,070(11)$ and $(\delta R/R)^{40,42} = 1.0 \times 10^{-8}$. This result arises from 11 data points and is less precise than the one from the literature, $(\delta R/R)_{\text{lit}}^{40,42} = 3.9 \times 10^{-9}$. With the current performance of our system, one would need about 80 data points to reach the same level of precision. Our result of $R^{40,48} = 1.199\,938\,029(15)$ with $(\delta R/R)^{40,48} = 1.3 \times 10^{-8}$ (based on 26 data points) is also in agreement with the quoted value $R_{\text{lit}}^{40,48} = 1.199\,938\,024\,55(81)$, but with much lower precision than $(\delta R/R)_{\text{lit}}^{40,48} = 6.8 \times 10^{-10}$ (see Ref. [33] and Supplemental Material [34]). $^{48}\text{Ca}^+$ has been measured with several Penning traps by means of destructive detection techniques, yielding better precision than in this work [35–37]. Reaching the same uncertainty level using the optical detector would demand an increase of $t_{\text{dip}}^{+,z}$ by a factor of ~ 35 and, implicitly, the use of DC power supplies with higher stability.

Our method provides the direct observation of the radial motions, allowing for a fine tuning of amplitudes of the target and reference ion to reduce the systematic deviation due to the mass difference. Figure 3 shows histograms for $\Delta v_c/v_c$ from the amplitudes of the ions' eigenmotions (ρ_u in Fig. 2), in units of c_4/c_2 and b_2/b_0 [38]. Our results are also compared with our calculations from the estimated ion's

oscillation amplitudes in other experiments [39,40]. Note that in the case of Ref. [40], the charge state of the ions is $+17$. This leads to larger eigenfrequencies and a better value of $\Delta v_c/v_c \sim 4 \times 10^{-9}$ in c_4/c_2 units than the one shown in Fig. 3 (1.1×10^{-6}), scaled for an ion with $m/q \sim 40$. Our uncertainty due to image charges is estimated to be 9×10^{-11} in v_c and 2×10^{-11} in R in the worst case. The uncertainty due to relativistic effects is negligible, with a maximum from our measurements of 1.2×10^{-13} (in v_c).

The use of this ion-based detector in Penning-trap mass spectrometry requires only small ion-motional amplitudes, and thus very tiny fields for detection. The minimum amplitude utilized in our experiments to obtain a full resonance curve allows us to extract a force sensitivity of $50(14)$ yN/ $\sqrt{\text{Hz}}$ when $\nu_{\text{dip}} = \nu_+$ [Fig. 1(d)], with a signal-to-noise ratio (SNR) of 6.8(1.3). This value has been obtained from $F_r = 2m\omega_1\rho_+/t_{\text{dip}}^+$ with $\omega_1 = \sqrt{\omega_c^2 - \omega_z^2}$, using the measured value of ρ_+ within $t_{\text{dip}}^+ = 1$ s + $t_{\text{EMCCD}} = 75$ ms. In the axial direction, $F_z = 2m\omega_z\rho_z/t_{\text{dip}}^z$, and the sensitivity achieved for a SNR = 3.9(5) is $97(26)$ yN/ $\sqrt{\text{Hz}}$ ($t_{\text{dip}}^z = 100$ ms + $t_{\text{PMT}} = 75$ ms). These values can be improved by orders of magnitude if the ion is cooled to the ground state of motion, overcoming the best value of $5.76(24)$ yN/ $\sqrt{\text{Hz}}$ at 1.59 MHz using quantum protocols [2], as can be inferred from measurements of single quantum jumps in the modified-cyclotron frequency of an electron [41].

Improving the sensitivity in the Doppler limit by a factor of 4–5 will result in a considerable improvement in the accuracy, as shown in Fig. 3 (UGR at Doppler limit). This can be accomplished by reducing the intensities and waists of the cooling laser beams, once the stability of the DC power supplies has been improved. A long-term stability of 4.5×10^{-5} is obtained from measurements of the magnetron frequency. The magnetic field, however, is stable on the level of precision in reach in this Letter (see Supplemental Material [34]). Measurements with longer t_{dip}^u will result in cyclotron frequencies with the precision envisaged for experiments aiming at determining the modes' eigenfrequencies of an unbalanced Coulomb crystal ($^{40}\text{Ca}^+ - \text{X}^{n+}$) at the lowest temperature [24].

We acknowledge support from Ministerio de Ciencia, Innovación y Universidades through Grant No. PID2022-141496NB-I00 funded by MCIN/AEI/10.13039/501100011033 and by ERDF A way of making Europe, and Grant No. PID2019-104093GB-I00 funded by MCIN/AEI/10.13039/501100011033, from FEDER/Junta de Andalucía- Consejería de Universidad, Investigación e Innovación through Project No. P18-FR-3432, from the Spanish Ministry of Education through Ph.D. fellowship FPU17/02596, and from the University of Granada “Laboratorios Singulares 2020.” The construction of the facility was supported by the European Research Council (Contract No. 278648-TRAPSENSOR), Projects No. FPA2015-67694-P (funded by MCIN/AEI/10.13039/501100011033 and by ERDF A way of making Europe) and No. FPA2012-32076 (MCIN/FEDER), infrastructure Projects No. UNGR10-1E-501, and No. UNGR13-1E-1830

(MCIN/FEDER/UGR), and No. EQC2018-005130-P (funded by MCIN/AEI/10.13039/501100011033 and by ERDF A way of making Europe), and infrastructure Projects No. INF-2011-57131 and No. IE2017-5513 (funded by

Junta de Andalucía/FEDER). I.A. acknowledges support from the European Union's Horizon 2020 research and innovation program under Grant Agreement No. 899354 (SuperQuLAN).

- [1] M. J. Biercuk, H. Uys, J. W. Britton, A. P. VanDevender, and J. J. Bollinger, Ultrasensitive detection of force and displacement using trapped ions, *Nat. Nanotechnol.* **5**, 646 (2010).
- [2] K. A. Gilmore, M. Affolter, R. J. Lewis-Swan, D. Barberena, E. Jordan, A. M. Rey, and J. J. Bollinger, Quantum-enhanced sensing of displacements and electric fields with two-dimensional trapped-ion crystals, *Science* **373**, 673 (2021).
- [3] E. G. Myers, High-precision atomic mass measurements for fundamental constants, *Atoms* **7**, 37 (2019).
- [4] S. Ulmer, C. Smorra, A. Mooser, K. Franke, H. Nagahama, G. Schneider, T. Higuchi, S. Van Gorp, K. Blaum, Y. Matsuda, W. Quint, J. Walz, and Y. Yamazaki, High-precision comparison of the antiproton-to-proton charge-to-mass ratio, *Nature (London)* **524**, 196 (2015).
- [5] E. G. Myers, *CPT* tests with the antihydrogen molecular ion, *Phys. Rev. A* **98**, 010101(R) (2018).
- [6] S. Rainville, J. K. Thompson, and D. E. Pritchard, An ion balance for ultra-high-precision atomic mass measurements, *Science* **303**, 334 (2004).
- [7] S. Rainville Jr, J. K. Thompson, E. G. Myers, J. M. Brown, M. S. Dewey, E. G. Kessler, R. D. Deslattes, H. G. Börner, M. Jentschel, P. Mutti, and D. E. Pritchard, A direct test of $E = mc^2$, *Nature (London)* **438**, 1096 (2005).
- [8] E. G. Myers, A. Wagner, H. Kracke, and B. A. Wesson, Atomic masses of tritium and helium-3, *Phys. Rev. Lett.* **114**, 013003 (2015).
- [9] R. X. Schüssler, H. Bekker, M. Brass, H. Cakir, J. R. C. López-Urrutia, M. Door, P. Filianin, Z. Harman, M. W. Haverkort, W. J. Huang, P. Indelicato, C. H. Keitel, C. M. König, K. Kromer, M. Müller, Y. N. Novikov, A. Rischka, C. Schweiger, S. Sturm, S. Ulmer *et al.*, Detection of metastable electronic states by Penning trap mass spectrometry, *Nature (London)* **581**, 42 (2020).
- [10] D. J. Wineland and H. G. Dehmelt, Principles of the stored ion calorimeter, *J. Appl. Phys.* **46**, 919 (1975).
- [11] L. S. Brown and G. Gabrielse, Geonium theory: Physics of a single electron or ion in a Penning trap, *Rev. Mod. Phys.* **58**, 233 (1986).
- [12] P. Filianin, C. Lyu, M. Door, K. Blaum, W. J. Huang, M. Haverkort, P. Indelicato, C. H. Keitel, K. Kromer, D. Lange, Y. N. Novikov, A. Rischka, R. X. Schüssler, C. Schweiger, S. Sturm, S. Ulmer, Z. Harman, and S. Eliseev, Direct Q -value determination of the β^- decay of ^{187}Re , *Phys. Rev. Lett.* **127**, 072502 (2021).
- [13] R. M. Weisskoff, G. P. Lafyatis, K. R. Boyce, E. A. Cornell, R. W. Flanagan, and D. Pritchard, rf SQUID detector for single-ion trapping experiments, *J. Appl. Phys.* **63**, 4599 (1988).
- [14] S. Ulmer, H. Kracke, K. Blaum, S. Kreim, A. Mooser, W. Quint, C. C. Rodegheri, and J. Walz, The quality factor of a superconducting rf resonator in a magnetic field, *Rev. Sci. Instrum.* **80**, 123302 (2009).
- [15] E. A. Cornell, R. M. Weisskoff, K. R. Boyce, and D. E. Pritchard, Mode coupling in a Penning trap: π pulses and a classical avoided crossing, *Phys. Rev. A* **41**, 312 (1990).
- [16] D. J. Wineland, J. J. Bollinger, and W. M. Itano, Laser-fluorescence mass spectroscopy, *Phys. Rev. Lett.* **50**, 628 (1983).
- [17] H. M. Imajo, S. Urabe, K. Hayasaka, and M. Watanabe, Measurements of motional frequencies for laser-cooled ions in a penning trap, *J. Mod. Opt.* **39**, 317 (1992).
- [18] B. J. McMahon, C. Volin, W. G. Rellergert, and B. C. Sawyer, Doppler-cooled ions in a compact reconfigurable Penning trap, *Phys. Rev. A* **101**, 013408 (2020).
- [19] S. Nagy, T. Fritioff, A. Solders, R. Schuch, M. Björkhage, and I. Bergström, Precision mass measurements of $^{40}\text{Ca}^{17+}$ and $^{40}\text{Ca}^{19+}$ ions in a Penning trap, *Eur. Phys. J. D* **39**, 1 (2006).
- [20] F. Gebert, Y. Wan, F. Wolf, C. N. Angstmann, J. C. Berengut, and P. O. Schmidt, Precision isotope shift measurements in calcium ions using quantum logic detection schemes, *Phys. Rev. Lett.* **115**, 053003 (2015).
- [21] F. W. Knollmann, A. N. Patel, and S. C. Doret, Part-per-billion measurement of the $4^2S_{1/2} \rightarrow 3^2D_{5/2}$ electric-quadrupole-transition isotope shifts between $^{42,44,48}\text{Ca}^+$ and $^{40}\text{Ca}^+$, *Phys. Rev. A* **100**, 022514 (2019).
- [22] C. Solaro, S. Meyer, K. Fisher, J. C. Berengut, E. Fuchs, and M. Drewsen, Improved isotope-shift-based bounds on bosons beyond the standard model through measurements of the $^2D_{3/2} - ^2D_{5/2}$ interval in Ca^+ , *Phys. Rev. Lett.* **125**, 123003 (2020).
- [23] M. J. Gutiérrez, J. Berrocal, F. Domínguez, I. Arrazola, M. Block, E. Solano, and D. Rodríguez, Dynamics of an unbalanced two-ion crystal in a Penning trap for application in optical mass spectrometry, *Phys. Rev. A* **100**, 063415 (2019).
- [24] J. Cerrillo and D. Rodríguez, Motional quantum metrology in a Penning trap, *Europhys. Lett.* **134**, 38001 (2021).
- [25] M. Block, D. Ackermann, K. Blaum, C. Droese, M. Dworschak, S. Eliseev, T. Fleckenstein, E. Haettner, F. Herfurth, F. P. Heßberger, S. Hofmann, J. Ketelaer, J. Ketter, H.-J. Kluge, G. Marx, M. Mazzocco, Y. N. Novikov, W. R. Plaß, A. Popeko, S. Rahaman *et al.*, Direct mass measurements above uranium bridge the gap to the island of stability, *Nature (London)* **463**, 785 (2010).
- [26] E. M. Ramirez, D. Ackermann, K. Blaum, M. Block, C. Droese, Ch. E. Düllmann, M. Dworschak, M. Eibach, S. Eliseev, E. Haettner, F. Herfurth, F. P. Heßberger, S. Hofmann, J. Ketelaer, G. Marx, M. Mazzocco, D. Nesterenko, Yu. N. Novikov, W. R. Plaß, D. Rodríguez *et al.*, Direct mapping of nuclear shell effects in the heaviest elements, *Science* **337**, 1207 (2012).
- [27] O. Kaleja, B. Andelić, O. Bezrodnova, K. Blaum, M. Block, S. Chenmarev, P. Chhetri, C. Droese, C. E. Düllmann, M. Eibach, S. Eliseev, J. Even, P. Filianin, F. Giacoppo, S. Götz, Y. Gusev, M. J. Gutiérrez, F. P. Hessberger, N. Kalantar-Nayestanaki, J. J. W. van de Laar *et al.*, Direct high-precision mass spec-

- trometry of superheavy elements with SHIPTRAP, *Phys. Rev. C* **106**, 054325 (2022).
- [28] M. J. Gutiérrez, J. Berrocal, J. M. Cornejo, F. Domínguez, J. J. Del Pozo, I. Arrazola, J. Bañuelos, P. Escobedo, O. Kaleja, L. Lamata, R. A. Rica, S. Schmidt, M. Block, E. Solano, and D. Rodríguez, The TRAPSENSOR facility: An open-ring 7 tesla Penning trap for laser-based precision experiments, *New J. Phys.* **21**, 023023 (2019).
- [29] J. Berrocal, E. Altozano, F. Domínguez, M. J. Gutiérrez, J. Cerrillo, F. J. Fernández, M. Block, C. Ospelkaus, and D. Rodríguez, Formation of two-ion crystals by injection from a Paul-trap source into a high-magnetic-field Penning trap, *Phys. Rev. A* **105**, 052603 (2022).
- [30] D. R. Crick, S. Donnellan, D. M. Segal, and R. C. Thompson, Magnetically induced electron shelving in a trapped Ca^+ ion, *Phys. Rev. A* **81**, 052503 (2010).
- [31] H. F. Powell, D. M. Segal, and R. C. Thompson, Axialization of laser cooled magnesium ions in a penning trap, *Phys. Rev. Lett.* **89**, 093003 (2002).
- [32] SIMION[®] 8.0 Ion and Electron Optics Simulator <https://simion.com/>.
- [33] M. Wang, W. Huang, F. Kondev, G. Audi, and S. Naimi, The AME 2020 atomic mass evaluation (II). Tables, graphs and references, *Chin. Phys. C* **45**, 030003 (2021).
- [34] See Supplemental Material at <http://link.aps.org/supplemental/10.1103/PhysRevResearch.6.L012001> for the measurements used to determine $R_{\text{lit}}^{40,48}$, presented analogously as in Fig. 2; the eigenfrequency data used to obtain the ratios shown in Fig. 2; and a discussion about the electric-field noise and the magnetic-field stability based on a correlation analysis of the eigenfrequencies. It also contains Ref. [33].
- [35] S. Bustabad, G. Bollen, M. Brodeur, D. L. Lincoln, S. J. Novario, M. Redshaw, R. Ringle, S. Schwarz, and A. A. Valverde, First direct determination of the ^{48}Ca double- β decay Q value, *Phys. Rev. C* **88**, 022501(R) (2013).
- [36] A. A. Kwiatkowski, T. Brunner, J. D. Holt, A. Chaudhuri, U. Chowdhury, M. Eibach, J. Engel, A. T. Gallant, A. Grossheim, M. Horoi, A. Lennarz, T. D. Macdonald, M. R. Pearson, B. E. Schultz, M. C. Simon, R. A. Senkov, V. V. Simon, K. Zuber, and J. Dilling, New determination of double- β -decay properties in ^{48}Ca : High-precision $Q_{\beta\beta}$ -value measurement and improved nuclear matrix element calculations, *Phys. Rev. C* **89**, 045502 (2014).
- [37] F. Köhler, K. Blaum, M. Block, S. Chenmarev, S. Eliseev, D. A. Glazov, M. Goncharov, J. Hou, A. Kracke, D. A. Nesterenko, Y. N. Novikov, W. Quint, E. Minaya-Ramirez, V. M. Shabaev, S. Sturm, A. V. Volotka, and G. Werth, Isotope dependence of the Zeeman effect in lithium-like calcium, *Nat. Commun.* **7**, 10246 (2016).
- [38] J. Ketter, T. Eronen, M. Höcker, S. Streubel, and K. Blaum, First-order perturbative calculation of the frequency-shifts caused by static cylindrically-symmetric electric and magnetic imperfections of a Penning trap, *Intl. J. Mass Spectrom.* **358**, 1 (2014).
- [39] M. Redshaw, Precise measurements of the atomic masses of ^{28}Si , ^{31}P , ^{32}S , $^{84,86}\text{Kr}$, $^{129,132,136}\text{Xe}$, and the dipole moment of Ph^+ using single-ion and two-ion penning trap techniques, Ph.D. thesis, Florida State University, 2007.
- [40] R. Schüssler, First high-precision mass measurements at penta-trap on highly charged Xe and Re ions, Ph.D. thesis, University of Heidelberg, 2019.
- [41] X. Fan, T. G. Myers, B. A. D. Sukra, and G. Gabrielse, Measurement of the electron magnetic moment, *Phys. Rev. Lett.* **130**, 071801 (2023).